The Astrophysical Journal, 603:729–737, 2004 March 10

OTHER KUIPER BELTS

M. Jura
Department of Physics and Astronomy, University of California, Los Angeles CA 90095-1562; jura@clotho.astro.ucla.edu
Received 2003 July 9; accepted 2003 November 21

ABSTRACT

When a main sequence star evolves into a red giant and its Kuiper Belt objects (KBOs) reach a temperature of $\sim$170 K, the dust released during the rapid ice sublimation of these cometary bodies may lead to a detectable infrared excess at 25 μm, depending on the mass of the KBOs. Analysis of *IRAS* data for 66 first-ascent red giants with 200 $L_\odot < L <$ 300 $L_\odot$ within 150 pc of the Sun provides an upper limit to the mass in KBOs at 45 AU orbital radius that is usually less than $\sim$0.1 $M_\oplus$. With improved infrared data, we may detect systems of KBOs around first-ascent red giants that are analogs to our solar system.

Subject headings: circumstellar matter — comets: general

1. INTRODUCTION

The formation and evolution of large solids such as comets, asteroids, and planets in astrophysical environments is of great interest. Here, we investigate whether other stars possess Kuiper Belt objects (KBOs) similar to those found in the solar system.

We assume that the hypothetical KBOs around other stars resemble those in our solar system and have a composition of ice and dust similar to that of comets (see Luu & Jewitt 2002). During the main-sequence phase of the star's evolution, the KBOs quiescently remain in stable orbits. However, when the star becomes a red giant, the KBOs become sufficiently hot that ice sublimates and previously embedded dust particles are ejected into the surroundings. In § 2, we sketch our argument, which is presented in full detail in § 3, that sufficient dust may be released during this red giant phase that the star can display a detectable infrared excess.

Stern, Shull, & Brandt (1990) and Ford & Neufeld (2001) computed the fate of ice sublimated from comets with orbital radii greater than 100 AU after the host star evolves onto the asymptotic giant branch and attains a luminosity near 10^4 $L_\odot$. Now that the Kuiper Belt in the solar system, which has most of its objects lying near 45 AU from the Sun, is becoming better understood (Luu & Jewitt 2002), it is possible to imagine the response of such a system to a star's first ascent up the red giant branch when L_* exceeds 100 $L_\odot$. However, although progress is being made, there are still significant uncertainties about the Kuiper Belt in the solar system. Recent estimates of its mass range from 0.01 (Bernstein et al. 2003) to 0.1 $M_\oplus$ (Luu & Jewitt 2002). Therefore, although we describe a procedure to investigate Kuiper Belt–like systems around other stars, our own outer solar system is so poorly understood that an exact comparison is not yet possible.

Two current descriptions of the KBOs differ mainly, but not exclusively, in estimates of the numbers of objects with radii smaller than $\sim$200 km. With the expectation that short-period comets originate in the Kuiper Belt, Luu & Jewitt (2002) propose a rapid rise in the numbers of such smaller KBOs. In contrast to this expectation, Bernstein et al. (2003) used the *Hubble Space Telescope* to search for KBOs as faint as 28.3 mag, which corresponds to radii of $\sim$15 km, and found many fewer objects than expected from the model given by Luu & Jewitt (2002). With this observational result, the origin of the short-period comets becomes a mystery. Perhaps there is a bimodal distribution of KBOs. In this paper, given the uncertainties in current knowledge of the outer solar system, we consider models both with and without large numbers of KBOs smaller than 200 km in radius.

Most first-ascent red giants do not show any evidence for circumstellar dust. The minority of first-ascent red giants that do exhibit infrared excesses (Judge, Jordan, & Rowan-Robinson 1987; Jura 1990, 1999; Kim, Zuckerman, & Silverstone 2001; Smith 1998; Zuckerman, Kim, & Liu 1995; Plets et al. 1997) do not seem to have sublimating KBOs, since the characteristic inferred dust temperature is less than 70 K instead of 170 K, as we predict in § 3. Here, we focus on the possibility of detecting relatively warm dust from disintegrating KBOs.

2. OVERVIEW

Because the details of our model are somewhat complicated, we first present a schematic overview of our analysis, while the complete description is presented in § 3. Using our own Kuiper Belt as a prototype, we assume that the KBOs orbit the host star near 45 AU. At this orbital separation, we find that most of the KBO material survives in the solid phase as long as the temperature is less than $\sim$150 K, which occurs as long as the star is less luminous than $\sim$170 $L_\odot$. However, once the star's luminosity exceeds this value, the KBOs become warm enough that relatively rapid ice sublimation occurs. In the time interval, approximately characterized by the parameter $t_{\rm RGB}$, during which the star increases in luminosity from $\sim$170 to $\sim$300 $L_\odot$, most of the mass of the KBOs is lost into their surroundings. As the KBOs are sublimating, some dust particles are released that continue to orbit the star. If sufficient mass is released from the KBOs, these orbiting dust grains can absorb enough light to produce a detectable infrared excess.

If $M_{\rm KBO}(0)$ denotes the total initial mass of the KBOs and $f_{\rm orbit}$ denotes the fraction of this mass that is ejected as dust particles that are large enough to remain in orbit around the star and are not blown out of the system by radiation pressure, then the total amount of mass that can orbit the star is $f_{\rm orbit}\, M_{\rm KBO}(0)$. We assume that the dust particles are spheres of radius b and density $\rho_{\rm dust}$ and that they orbit the star of luminosity L_* at distance D. While this assumption is relaxed in § 3.7, here, for simplicity, we assume that D does not change during a dust particle's evolution. Also, while other factors are considered in

§ 3.7, here we assume that the lifetime of the orbiting dust particles is controlled simply by the Poynting-Robertson time, t_{PR}. Following Burns, Lamy, & Soter (1979), we write

$$t_{PR} = \frac{4\pi b \rho_{dust} c^2 D^2}{3 L_*}. \quad (1)$$

Since the Poynting-Robertson lifetime is typically shorter than the characteristic evolutionary time on the red giant branch, at any given moment during the star's evolutionary phase when grains are being released, the fraction of orbiting material contributing to the infrared excess is t_{PR}/t_{RGB}. If the grains have opacity χ (cm^2 g^{-1}) and if the circumstellar dust cloud is optically thin, then the total luminosity of the circumstellar dust, L_{excess}, is scaled from the fractional dust coverage of an imaginary sphere of surface area $4\pi D^2$ by the relationship

$$L_{excess} \approx \left[\frac{\chi f_{orbit} M_{KBO}(0)}{4\pi D^2}\right]\left(\frac{t_{PR}}{t_{RGB}}\right) L_*. \quad (2)$$

We use a simple model of the grain opacity in which the geometric cross section πb^2 equals the total absorption cross section. In this case, since each dust grain has mass $4\pi\rho_{dust} b^3/3$, we can write

$$\chi = \frac{3}{4\rho_{dust} b}. \quad (3)$$

Combining equations (1)–(3), we find

$$L_{excess} \approx \frac{f_{orbit} M_{KBO}(0) c^2}{4 t_{RGB}}. \quad (4)$$

Expression (4) captures the essence of our model. The infrared luminosity simply scales as the rate of production of dust grains, which varies as $M_{KBO}(0)/t_{RGB}$. If f_{orbit} and $M_{KBO}(0)$ are sufficiently large, then the infrared excess may be detectable. Our estimate of L_{excess}, which is computed more exactly in § 3, is independent of the size of the KBOs, as long as these objects are fully destroyed by sublimation.

In § 3, we find characteristic values of $f_{orbit} \approx 0.25$ and $t_{RGB} \approx 14$ Myr. Therefore, if $M_{KBO}(0) \sim 0.1\ M_\oplus$, then from equation (4), $L_{excess} \approx 0.02\ L_\odot$. Because the KBOs mostly sublimate near 170 K, the spectrum of this excess luminosity peaks at wavelengths near 25 μm. In § 4, we show that a 170 K blackbody with a luminosity of $0.02\ L_\odot$ is just at the threshold of having been detected with *IRAS* data for red giants with total luminosities less than 300 $L_\odot$. Consequently, the absence of a measurable infrared excess at 25 μm around these red giants can be used to place an upper limit to the mass of KBOs closer than $\sim$50 AU of $\sim 0.1\ M_\oplus$. In § 5, we discuss our results and in § 6, we present our conclusions.

3. DETAILED MODEL

We now elaborate about the schematic model described in § 2. To compute the fate of the KBOs when a star is evolving as a red giant, we write for the total mass loss rate from KBOs, $\dot{M}_{KBO}$, that

$$\dot{M}_{KBO} = \dot{\sigma}_{KBO}(T) A_{KBO}(t). \quad (5)$$

In equation (5), $\dot{\sigma}_{KBO}$ denotes the mass loss rate per unit surface area of the KBOs as a function of temperature T, while $A_{KBO}(t)$ denotes the total surface area of these objects as a function of time t. In § 3.3 and § 3.4, we describe calculations for $\dot{\sigma}_{KBO}$ and A_{KBO} as functions of time or temperature, and we show in § 3.7 how $\dot{M}_{KBO}$ can be used to estimate the infrared excess.

3.1. *Initial Mass and Total Area of the KBOs*

Here, we consider two size distributions: systems with initially many small (radius less than 200 km) KBOs and Kuiper belts with initially no KBOs smaller than 200 km in radius.

3.1.1. *Model with Initially Many Small KBOs*

Following Luu & Jewitt (2002), we assume the KBOs are icy spheres of radius a and follow a broken power law for the size distribution $n(a)da$. For $a > a_{break}$,

$$n(a)da = n_0 \left(\frac{a_{break}}{a}\right)^4 da, \quad (6)$$

while for $a < a_{break}$,

$$n(a)da = n_0 \left(\frac{a_{break}}{a}\right)^{3.5} da. \quad (7)$$

From Luu & Jewitt (2002), we take $a_{break} = 1$ km and a maximum size, a_{max}, of about 1000 km. The distribution in equation (7) for the KBOs smaller than 1 km is derived from theoretical models (Kenyon 2002) and is consistent with upper limits of the contribution of KBOs to the zodiacal light and to distortions of the microwave background (Kenyon & Windhorst 2001; Teplitz et al. 1999).

Before a star becomes a red giant, the initial mass of the larger KBOs, $M_{large}(0)$, is

$$M_{large}(0) = \int_{a_{break}}^{a_{max}} n_0 \left(\frac{a_{break}}{a}\right)^4 \left(\frac{4\pi\rho_{KBO} a^3}{3}\right) da = \frac{4\pi}{3}\rho_{KBO} n_0 a_{break}^4 \ln\left(\frac{a_{max}}{a_{break}}\right), \quad (8)$$

where ρ_{KBO} denotes the density of the KBOs. Following Greenberg (1998) and Kenyon (2002), we assume that the KBOs are composed mostly of ice with some additional refractory dust and that $\rho_{KBO} = 1.5$ g cm^{-3}. From the measured size distribution of KBOs (Luu & Jewitt 2002), we adopt $M_{large}(0) = 0.1\ M_\oplus$ as a first approximation to the mass of KBOs. Luu & Jewitt (2002) use $\rho_{KBO} = 1.0$ g cm^{-3} and a slightly smaller total mass of $0.08\ M_\oplus$.

The total initial surface area of the large KBOs, $A_{large}(0)$, is

$$A_{large}(0) = \int_{a_{break}}^{a_{max}} n_0 \left(\frac{a_{break}}{a}\right)^4 (4\pi a^2)\, da \approx 4\pi n_0 a_{break}^3 \approx \frac{3 M_{large}(0)}{\rho_{KBO} a_{break} \ln(a_{max}/a_{break})}. \quad (9)$$

For the parameters we adopted above, $A_{large}(0) = 1.7 \times 10^{21}$ cm^2.

We can also compute the total mass contained in the KBOs with a smaller than 1 km. If a_{min} denotes the smallest KBO, then

$$M_{small}(0) = \int_{a_{min}}^{a_{break}} n_0 \left(\frac{a_{break}}{a}\right)^{3.5} \left(\frac{4\pi\rho_{KBO} a^3}{3}\right) da \approx \frac{8\pi}{3}\rho_{KBO} n_0 a_{break}^4. \quad (10)$$

As long as $a_{min} \ll a_{break}$, then evaluation of the integral in equation (10) shows that the mass of the small KBOs is essentially independent of a_{min}. From equations (8) and (10),

we find that

$$M_{\rm small}(0) = \frac{2M_{\rm large}(0)}{\ln(a_{\rm max}/a_{\rm break})}. \quad (11)$$

Therefore, with our adopted values of $a_{\rm max}$ and $a_{\rm break}$, we find that $M_{\rm small}(0) \approx 0.3 M_{\rm large}(0)$; most of the mass of the KBOs is contained in the larger objects.

3.1.2. *Model with Initially Only Large KBOs*

As a second model, we adopt a simplified version of the results of Bernstein et al. (2003). In particular, we assume that the size distribution of KBOs follows equation (6) but that there are no KBOs smaller than $a_{\rm break}$ with $a_{\rm break} = 200$ km instead of 1 km. We denote the initial mass of the KBOs in this system as $M_{\rm big}(0)$. If the numbers of objects larger than 200 km in radius is the same as in the model described in § 3.1.1, then $M_{\rm big}(0) \approx 0.02\ M_\oplus$. Although this model is representative of the results of Bernstein et al. (2003), it does not agree exactly with their description of the Kuiper Belt. One source of uncertainty is that, even for KBOs larger than 200 km in radius, there are some differences between the descriptions of Luu & Jewitt (2002) and Bernstein et al. (2003) that we cannot resolve in this paper. In any case, by evaluating the integral in equation (9) with the new lower limit to the size of 200 km, we find that the initial area of the KBOs in this model, $A_{\rm big}(0)$, is 8.7×10^{18} cm^2.

3.2. *Red Giant Branch Evolution*

The fate of a KBO is controlled by the host star's evolution. For simplicity, we parameterize the detailed calculations by Girardi et al. (2000) for a star's luminosity, L_*, on the red giant branch as

$$L_*(t) \approx L_0 e^{t/t_{\rm RGB}}. \quad (12)$$

For stars of 1 $M_\odot$, we fitted equation (12) with $t_{\rm RGB} = 1.4 \times 10^7$ yr, $L_0 = 87\ L_\odot$ and a starting time ($t = 0$) of 1.220×10^{10} yr after the star's birth. For stars with 1.5 $M_\odot$, we employ the same value of $t_{\rm RGB}$ and adopt a starting time of 2.7742×10^9 yr and $L_0 = 91\ L_\odot$. In Figure 1 we show a comparison of the prediction from equation (12) using $t_{\rm RGB} = 1.4 \times 10^7$ yr with the detailed calculations by Girardi et al. (2000) for stars of 1 and 1.5 $M_\odot$. For luminosities less than 1000 $L_\odot$, the agreement is usually better than 20%. Although equation (12) is an imperfect match to the detailed calculations, it does illustrate that the growth of luminosity with time on the red giant branch for a star of $\sim$150 $L_\odot$ is approximately an exponential with an e-folding time of $\sim 1.4 \times 10^7$ yr.

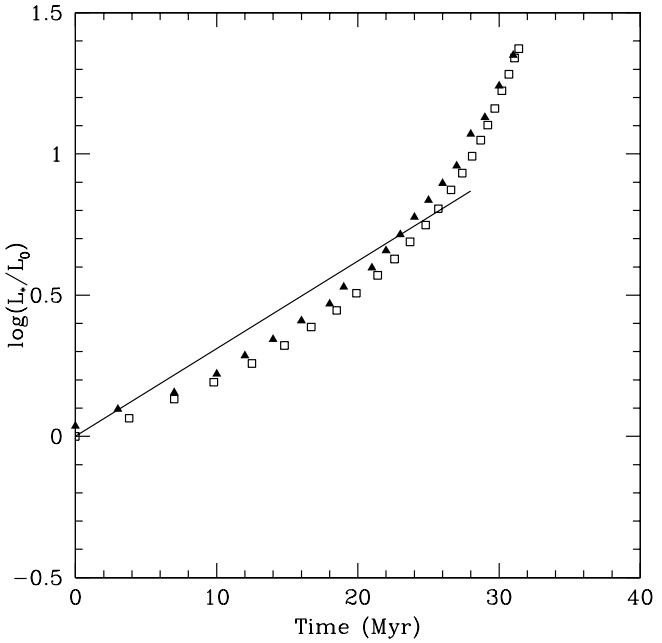

FIG. 1.—Theoretical calculations from Girardi et al. (2000) for the luminosity on the red giant branch vs. time. The filled triangles show the results for a star of 1 $M_\odot$, $L_0 = 87\ L_\odot$, and a starting time of 1.220×10^{10} yr, while the open squares show the calculations for a star of 1.5 $M_\odot$, $L_0 = 91\ L_\odot$, and a starting time of 2.7742×10^9 yr. The solid line shows the prediction from eq. (12) for $t_{\rm RGB} = 14$ Myr. The solid curve lies within 20% of the detailed calculations for $L < 1000\ L_\odot$ for both sets of models.

3.3. *Ice Sublimation*

With the description given in § 3.2 of the star's evolution, we can estimate the rate of ice sublimation from an individual KBO. We start with the expression

$$\frac{d}{dt}\frac{4\pi\rho_{\rm KBO}a^3}{3} = -4\pi a^2 \dot{\sigma}_{\rm KBO}. \quad (13)$$

Therefore, at time t_f, the total decrease in the radius of a KBO, Δa, is given by the following solution to expression (13):

$$\Delta a(t_f) = \int_0^{t_f} \frac{\dot{\sigma}_{\rm KBO}[T(t)]}{\rho_{\rm KBO}}\, dt. \quad (14)$$

As in equation (5), T denotes the grain temperature. Note that Δa is independent of a.

To estimate $\dot{\sigma}_{\rm KBO}$, we follow Ford & Neufeld (2001) who denote this quantity as $\dot{m}$. Converting from the units they employ and using their expression for the vapor pressure of ice, we write that

$$\dot{\sigma}_{\rm KBO} = \dot{\sigma}_0 T^{-1/2} e^{-T_{\rm subl}/T}, \quad (15)$$

where $\dot{\sigma}_0 = 3.8 \times 10^8$ g cm^{-2} s^{-1} K$^{1/2}$ and $T_{\rm subl} = 5530$ K. In expression (15), the chemical binding energy of H_2O molecules onto the solid ice is $k_{\rm B}T_{\rm subl}$, where $k_{\rm B}$ is Boltzmann's constant.

To compute Δa from equation (14), we need to find the temperature of a KBO as a function of time. If we ignore the difference between the day and night side of the KBO, assume unit emissivity and an albedo of 0, which is close to 0.07, which may be a typical KBO albedo (Luu & Jewitt 2002), then, for a KBO at distance $D_{\rm init}$ from the star,

$$T(t) = \left[\frac{L_*(t)}{16\pi D_{\rm init}^2 \sigma_{\rm SB}}\right]^{1/4}, \quad (16)$$

where $\sigma_{\rm SB}$ is the Stefan-Boltzmann constant. In equation (16), we ignore cooling by sublimation. At 170 K, the characteristic temperature at which most of the ice has been sublimated, it can be shown from the results in Ford & Neufeld (2001) that cooling by ice sublimation is less than 7% of the cooling by radiation.

From equations (12) and (16), we write that

$$dt = 4t_{\rm RGB}\frac{dT}{T}. \quad (17)$$

Using equations (15) and (17), we rewrite equation (14) to find

$$\Delta a(T_f) = 4\frac{t_{\rm RGB}\dot{\sigma}_0}{\rho_{\rm KBO}}\int_0^{T_f} T^{-3/2}e^{-T_{\rm subl}/T}\,dT, \qquad (18)$$

where T_f is the KBOs temperature at time t_f. With the substitution that $u^2 = T_{\rm subl}/T$, the integral in equation (18) can be re-expressed as a complementary error function to give

$$\Delta a(T_f) = 8\frac{t_{\rm RGB}\dot{\sigma}_0}{\rho_{\rm KBO}T_{\rm subl}^{1/2}}\int_{u_f}^{\infty} e^{-u^2}\,du. \qquad (19)$$

When $u_f > 1$, which is equivalent to our case in which $T_{\rm subl} \gg T$, then (see, for example, Abramowitz & Stegun 1965)

$$\int_{u_f}^{\infty} e^{-u^2}\,du \approx \frac{1}{2}\frac{e^{-u_f^2}}{u_f}. \qquad (20)$$

Therefore,

$$\Delta a(T_f) \approx 4\frac{t_{\rm RGB}\dot{\sigma}_0}{\rho_{\rm KBO}}\frac{T_f^{1/2}}{T_{\rm subl}}e^{-T_{\rm subl}/T_f}. \qquad (21)$$

Equation (21) describes the shrinkage of KBOs as a function of their temperature. Numerically, for $T_f = 150$, 160, and 171 K, then $\Delta a = 1$, 10, and 100 km, respectively. These temperatures are achieved by KBOs at 45 AU, when the red giant's luminosity is 170, 220, and 290 $L_\odot$, respectively. Complete destruction of the KBOs is achieved when $\Delta a =$ 1000 km, which occurs for KBOs at 45 AU, when the star's luminosity is $\sim$400 $L_\odot$. In the model with initially many small KBOs at 45 AU orbital radius described in § 3.1.1, by the time the temperature attains $\sim$170 K, all the KBOs smaller than 100 km are destroyed and somewhat more than half of the total initial mass of KBOs has been sublimated. Therefore, we adopt 170 K as a characteristic reference temperature for production of dust from KBOs.

3.4. *Evolution of the Total Area of the KBOs*

Using our calculation for the evolution of the size of a single KBO, we now consider the evolution of the surface area of the entire ensemble to use in equation (5). Each KBO of initial radius a evolves into a KBO with radius a' where

$$a' = a - \Delta a(t). \qquad (22)$$

3.4.1. *Model with Initially Many Small KBOs*

For the large KBOs, we use equation (6) to find that their size distribution $n(a')da'$ is

$$n(a')da' = n_0\left(\frac{a_{\rm break}}{a' + \Delta a}\right)^4 da'. \qquad (23)$$

To evaluate the total area of the KBOs with time, there are two regimes to consider. If $\Delta a < a_{\rm break}$, we write that

$$A_{\rm large}(t) = \int_{a_{\rm break}-\Delta a}^{a_{\rm max}-\Delta a}(4\pi a'^2)n_0\left(\frac{a_{\rm break}}{a' + \Delta a}\right)^4 da'. \qquad (24)$$

Using equation (9), we evaluate expression (24) to find in the limit $a_{\rm max} \gg a_{\rm break}$ that

$$A_{\rm large}(t) = A_{\rm large}(0)\left(1 - \delta + \frac{\delta^2}{3}\right), \qquad (25)$$

where $\delta = \Delta a/a_{\rm break}$ and $A_{\rm large}(0)$ is taken from equation (9). From equation (25), we see that the total surface area of the large KBOs remains nearly constant until Δa approaches $a_{\rm break}$. Note that equation (25) is valid only when $\delta < 1$.

When $\Delta a > a_{\rm break}$, we must use a different lower bound in the integral, and we write that

$$A_{\rm large}(t) = \int_0^{a_{\rm max}-\Delta a}(4\pi a'^2)n_0\left(\frac{a_{\rm break}}{a' + \Delta a}\right)^4 da'. \qquad (26)$$

We evaluate equation (26) to find in the limit $a_{\rm max} \gg \Delta a$ that

$$A_{\rm large}(t) \approx A_{\rm large}(0)\frac{a_{\rm break}}{3\Delta a} = \frac{A_{\rm large}(0)}{3\delta}. \qquad (27)$$

Equation (27) is valid when $\delta > 1$. In this regime, the total area of the large KBOs decreases as Δa increases with time. As Δa approaches $a_{\rm max}$, equation (27) overestimates $A_{\rm large}(t)$. However, as long as $\Delta a < 0.5a_{\rm max}$, then we can find from equation (26) that equation (27) is accurate to better than a factor of 2.

In the above paragraph, we described the evolution with time of the total surface area of the KBOs initially larger than $a_{\rm break}$. In this paragraph, we describe the evolution of the surface area of the smaller KBOs. As long as $\Delta a > a_{\rm min}$, we can write from equation (7) that

$$A_{\rm small}(t) = \int_0^{a_{\rm break}-\Delta a}(4\pi a'^2)n_0\left(\frac{a_{\rm break}}{a' + \Delta a}\right)^{3.5} da'. \qquad (28)$$

Expression (28) can be conveniently evaluated to give

$$A_{\rm small}(t) = \frac{3M_{\rm small}(0)}{2\rho_{\rm KBO}(a_{\rm break}\Delta a)^{1/2}} \times \left[2(1-\delta^{1/2}) - \tfrac{4}{3}(1-\delta^{3/2}) + \tfrac{2}{5}(1-\delta^{5/2})\right]. \qquad (29)$$

Note that $A_{\rm small}$ approaches zero as Δa approaches $a_{\rm break}$, or, equivalently, as δ approaches unity.

3.4.2. *Model with Initially Only Large KBOs*

To calculate $A_{\rm big}(t)$, we simply substitute for $A_{\rm large}(t)$ in the equations in § 3.4.1 $a_{\rm break} = 200$ km instead of 1 km. When $\Delta a < a_{\rm break}$, we use equation (25), and when $\Delta a > a_{\rm break}$, we use equation (27).

3.5. *Total KBO Mass Loss Rate*

Armed with the KBO temperature and total surface area as functions of time, we can evaluate equation (5) to find the total rate at which KBOs lose mass into their surroundings. It is convenient to present $\dot{M}_{\rm KBO}$ as a function of the host star's luminosity, since that is a measurable quantity. The star's evolution is given by equation (12), and the sublimation rate from the KBOs is given by equation (15).

3.5.1. *Model with Initially Many Small KBOs*

For systems with many small KBOs, we consider two regimes for $\dot{M}_{\rm KBO}$ as a function of the star's luminosity. First, when $\Delta a > a_{\rm break}$, $A_{\rm large}(t)$ from equation (27) gives the total

surface area of the KBOs. In this case, $\dot{M}_{\rm KBO}$ reaches a saturation value and is nearly independent of L_*. At saturation, we find from equations (5), (9), (15), (21), and (27) that

$$\dot{M}_{\rm KBO}(T) = \left[\frac{1}{4\ln(a_{\rm max}/a_{\rm break})}\right]\left(\frac{T_{\rm subl}}{T}\right)\left[\frac{M_{\rm large}(0)}{t_{\rm RGB}}\right]. \quad (30)$$

Equation (30) shows that when $\Delta a > a_{\rm break}$, the sublimation rate from the KBOs depends mainly on the initial mass of the large KBOs and the timescale of the star's evolution on the red giant branch. In this phase, the rapid rise in the sublimation rate with temperature given in equation (15) is roughly balanced by the decrease in the total area of KBOs given in equation (27). When $T = 170$ K, we find from equation (30) that $\dot{M}_{\rm KBO} \approx 1.2 M_{\rm large}(0)/t_{\rm RGB}$, or 1.6×10^{12} g s^{-1}.

A second regime to consider is when $\Delta a < a_{\rm break}$. In this case, the total surface area of the KBOs is given by the sum of $A_{\rm large}(t)$ and $A_{\rm small}(t)$ from equations (25) and (29). In this regime, $\dot{M}_{\rm KBO}$ starts low and rises rapidly with the star's luminosity until saturation is achieved.

Graphical results for $\dot{M}_{\rm KBO}$ versus luminosity aare presented in Figure 2 for a model with $D_{\rm init} = 45$ AU and $M_{\rm large}(0) = 0.1\ M_\oplus$. For comparison, we also show the results for models with $D_{\rm init}$ of 40 and 50 AU. In all three cases, we see that $\dot{M}_{\rm KBO}$ approaches the saturation rate predicted by equation (30) for sufficiently large values of the star's luminosity.

3.5.2. *Model with Initially Only Large KBOs*

If initially there are only large KBOs, then, for much of the time during the star's evolution, the total surface area of the KBOs is approximately constant. As long as $\Delta a < 200$ km, we can write from equations (5), (15), and (25) that

$$\dot{M}_{\rm KBO}(T) = A_{\rm big}(0)\left(1 - \delta + \frac{\delta^2}{3}\right)\dot{\sigma}_0 T^{-1/2} e^{-T_{\rm subl}/T}. \quad (31)$$

Graphical results for $\dot{M}_{\rm KBO}$ versus luminosity from equations (30) and (31) are shown in Figure 2 for the case in which $D_{\rm init} = 45$ AU. We see that, for stellar luminosities less than $\sim$300 $L_\odot$, the dust production rate is relatively small in this regime for which initially there are only large KBOs, but as the luminosity increases, the saturation value of $\dot{M}_{\rm KBO}$ is attained.

3.6. *Dust Production*

In § 3.5, we estimated the rate at which ice sublimates from the KBOs; here, we estimate the fractional mass of the KBOs released in dust that continues to orbit the star, $f_{\rm orbit}$. It is this orbiting dust that controls the infrared excess of the system.

It is plausible that half of the total mass of the KBOs is dust (Luu & Jewitt 2002) and that $f_{\rm orbit}$ could be as large as 0.5. However, we expect that $f_{\rm orbit}$ is less than 0.5, since dust grains that are smaller than a critical radius $b_{\rm crit}$, do not orbit the star of mass M_*, and instead are driven out the system by radiation pressure. The critical size for being gravitationally bound is (Artymowicz 1988)

$$b_{\rm crit} = \frac{3L_*}{16\pi\rho_{\rm dust} G M_* c}. \quad (32)$$

If the dust is composed of silicates with a density $\rho_{\rm dust}$, of 3 g cm^{-3}, then, for a 1 $M_\odot$ star of 300 $L_\odot$, the maximum luminosity that we consider, $b_{\rm crit} = 57\ \mu$m.

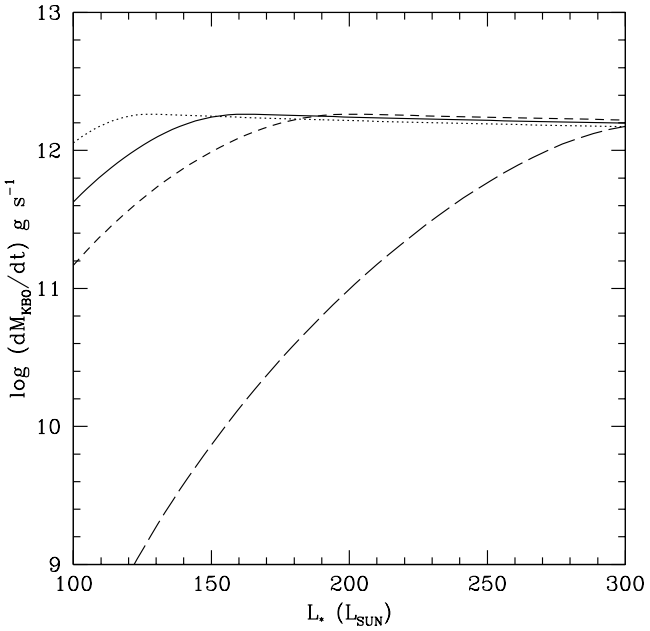

FIG. 2.—Mass loss rate $\dot{M}_{\rm KBO}$ from a cloud of KBOs vs. the star's luminosity. The solid line shows the calculations for the standard model consisting of both small and large KBOs with $D_{\rm init} = 45$ AU and $M_{\rm large}(0) = 0.1\ M_\oplus$, while the dotted and short-dashed lines show the results for the cases in which $D_{\rm init} = 40$ and 50 AU, respectively. Note the approach to saturation for $\dot{M}_{\rm KBO}$ given by equation (30). The long-dashed line shows the calculations from equation (31) for a cloud of only big KBOs with $M_{\rm big}(0) = 0.02\ M_\oplus$ at $D_{\rm init} = 45$ AU.

We assume that the size distribution of dust ejected from KBOs, $n_{\rm dust}(b)\ db$, resembles that of comets (Hanner, Veeder, & Tokunaga 1992; Harker et al. 2002; Li & Greenberg 1998), which we approximate as

$$n_{\rm dust} = n_C b^{-4} db. \quad (33)$$

We use $b_{\rm min}$ and $b_{\rm max}$ to denote the minimum and maximum size, respectively, of the dust from the KBOs, while n_C is a normalization constant, which does not matter for our purposes here. We may write that the total mass in the dust, $M_{\rm total}$ is

$$M_{\rm total} = \int_{b_{\rm min}}^{b_{\rm max}} \left(\frac{4\pi\rho_{\rm dust} b^3}{3}\right) n_C b^{-4}\, db. \quad (34)$$

Similarly, if $M_{\rm orbit}$ denotes the mass of the dust that is large enough to remain in orbit after it is produced, then

$$M_{\rm orbit} = \int_{b_{\rm crit}}^{b_{\rm max}} \left(\frac{4\pi\rho_{\rm dust} b^3}{3}\right) n_C b^{-4}\, db. \quad (35)$$

Since 0.5 of the mass of the KBOs is dust, we write that

$$f_{\rm orbit} = 0.5\frac{M_{\rm orbit}}{M_{\rm total}}. \quad (36)$$

Therefore, we find from equations (34)–(36) that

$$f_{\rm orbit} = 0.5\frac{\ln(b_{\rm crit}/b_{\rm min})}{\ln(b_{\rm max}/b_{\rm min})} \quad (37)$$

While the values of $b_{\rm min}$ and $b_{\rm max}$ are only poorly known, it seems for many comets that $b_{\rm min} \sim 0.1\ \mu$m and $b_{\rm max} \sim 1$ cm (see McDonnell et al. 1987; Hanner et al. 1992). Results from

meteorites (Kyte & Wasson 1986; Love & Brownlee 1995) and the *Long Duration Exposure Facility* (Zolensky et al. 1995) also show that many particles larger than 100 μm exist in the solar system. With these extrapolations from the solar system, we find from equation (37) that $f_{\rm orbit} \approx 0.25$.

3.7. *Infrared Excess*

We now elaborate on the schematic discussion given in § 2 to show that the infrared excess around a red giant, $L_{\rm excess}$, directly depends on the rate of dust production from the KBOs, $\dot{M}_{\rm KBO}$. Here, we include two additional physical processes not discussed in § 2 that control the grain's orbital evolution: stellar wind drag and grain-grain collisions.

The stellar wind drag is straightforward to incorporate into the model. Rewriting the notation of Gustafson (1994) and Burns et al. (1979), the increase by "drag" in the inward drift velocity over that produced by the Poynting-Robertson effect is given approximately by the factor $(1 + \dot{M}_{\rm wind}c^2/L_*)$, where $\dot{M}_{\rm wind}$ is the stellar wind mass loss rate. In the solar system, this drag created by the anisotropic recoil of solar wind particles off an orbiting dust grain typically scales as 0.3 of the Poynting-Robertson drag (see, for example, Gustafson 1994). Below, we argue that the stellar wind drag around red giants is of similar magnitude.

Consider now the orbital evolution of dust particles released from warmed-up KBOs. We assume that, as seen from the host star, the dust ejected from the sublimating KBOs is confined to a solid angle $\Omega_{\rm KBO}$. If the dust cloud is optically thin, the excess luminosity scales directly as the optical depth of the dust. If $n_{{\rm dust},i}$ denotes the density of dust particles of radius b_i, we write that

$$L_{\rm excess} = \left(\frac{\Omega_{\rm KBO}}{4\pi}\right) L_* \sum_i \int_{D_{\rm final}}^{D_{\rm init}} \pi b_i^2 n_{{\rm dust},i}(D)\, dD. \quad (38)$$

In equation (38), we assume that all the dust particles are formed at an initial outer distance from the star, $D_{\rm init}$, and they are all destroyed at some final, inner radius $D_{\rm final}$. We also assume that the cross section of the grains is simply given by their projected surface area πb_i^2.

We now show how the Poynting-Robertson and stellar wind drags affect the dust motion. From the equation of continuity, we write

$$n_{{\rm dust},i} = \frac{\dot{N}_{{\rm dust},i}}{\Omega_{\rm KBO} D^2 V_i(D)}, \quad (39)$$

where $\dot{N}_{{\rm dust},i}$ denotes the rate of production by number of dust grains from KBO sublimation and $V_i(D)$ denotes the inward radial drift speed of the same grains. If $\dot{M}_{{\rm dust},i}$ denotes the rate of production by mass of the ith type of particle, then

$$\dot{N}_{{\rm dust},i} = \frac{3\dot{M}_{{\rm dust},i}}{4\pi b_i^3 \rho_{\rm dust}}. \quad (40)$$

Since the dust particles drift inward under the action of the Poynting-Robertson drag, we write

$$V_i(D) = \left(\frac{3L_*}{8\pi b_i \rho_{\rm dust} c^2 D}\right)\left(1 + \frac{\dot{M}_{\rm wind}c^2}{L_*}\right) \quad (41)$$

(Burns et al. 1979; Gustafson 1994). Note that since $V = dD/dt$ and if we ignore the correction for stellar wind drag, equation (1) can be derived from equation (41).

We are now able to compute the infrared excess from the system. Combining equations (38)–(41), we find

$$L_{\rm excess} = \frac{1}{2}\sum_i \left[\dot{M}_{{\rm dust},i}c^2 \left(\int_{D_{\rm final}}^{D_{\rm init}} \frac{dD}{D}\right)\left(1 + \frac{\dot{M}_{\rm wind}c^2}{L_*}\right)^{-1}\right]. \quad (42)$$

From § 3.6, we write that

$$\sum_i \dot{M}_{{\rm dust},i} = \dot{M}_{\rm KBO} f_{\rm orbit}. \quad (43)$$

Therefore, evaluating equation (42) and using equation (43),

$$L_{\rm excess} = \frac{1}{2}\dot{M}_{\rm KBO}c^2 f_{\rm orbit} \times \left(1 + \frac{\dot{M}_{\rm wind}c^2}{L_*}\right)^{-1} \ln\left(\frac{D_{\rm init}}{D_{\rm final}}\right). \quad (44)$$

Equation (44) is a fundamental result in this paper and shows that the excess infrared luminosity scales directly as the dust production rate $\dot{M}_{\rm KBO}$.

It should be recognized that equation (44) is a more complex version of equation (4) derived in § 2. In equation (44), we employ $\dot{M}_{\rm KBO}$ instead of $M_{\rm KBO}(0)/t_{\rm RGB}$. Also, in equation (44), we include the wind contribution to limiting the particle's orbital lifetime, in addition to the Poynting-Robertson effect. Finally, there are numerical constants that are different between equations (4) and (44).

We now estimate the parameters required to use equation (44). First, we estimate the magnitude of the stellar wind drag. Currently, there are only a few first-ascent red giants for which the mass loss rate is measured with much confidence. Robinson, Carpenter, & Brown (1998) report L_* and $\dot{M}_{\rm wind}$ for α Tau (K5 III) and γ Dra (K5 III) of 394 $L_\odot$ and $\sim$1.3 $\times$ 10^{-11} $M_\odot$ yr^{-1} and 535 $L_\odot$ and $\sim$1.0 $\times$ 10^{-11} $M_\odot$ yr^{-1}, respectively. These results yield values of $\dot{M}_{\rm wind}c^2/L_*$ of 0.49 and 0.28, respectively. For HR 6902 (G2 II), the luminosity is 550 $L_\odot$ and $\dot{M}_{\rm wind}$ is somewhere between 0.8 and 3.4 $\times$ 10^{-11} $M_\odot$ yr^{-1} (Kirsch, Baade, & Reimers 2001). For this star, the correction to the Poynting-Robertson drag is between 0.2 and 0.9. Here, we simply assume that all red giants have the same stellar wind drag and adopt $\dot{M}_{\rm wind}c^2/L_* = 0.4$, a value close to that in the solar Ssystem.

To use equation (44), we also need to estimate $D_{\rm final}/D_{\rm init}$. In the absence of any other effects, the refractory dust would drift inward until it reached a temperature of $\sim$1000 K, when it would be destroyed by sublimation. From equation (16), we can show that if $T \sim 170$ K at $D_{\rm init}$, then $D_{\rm final} \sim 0.03 D_{\rm init}$. However, before they sublimate, the particles' orbits might be disrupted as they drift inward by grain-grain collisions. In such collisions, the grains may shatter into pieces, some of which are small enough to be driven away from the star by radiation pressure. Shattering may also produce more smaller grains with a net increase in surface area of the particles. If the radial optical depth through the circumstellar dust is τ, then, depending on the velocity dispersion of the grains and their size and spatial distributions, the probability during one orbital period P of a grain-grain collision may also be of order τ. Therefore, the mean time between collisions is P/τ. With an orbital period at 45 AU of 300 yr and $\tau = 10^{-4}$ (the optical

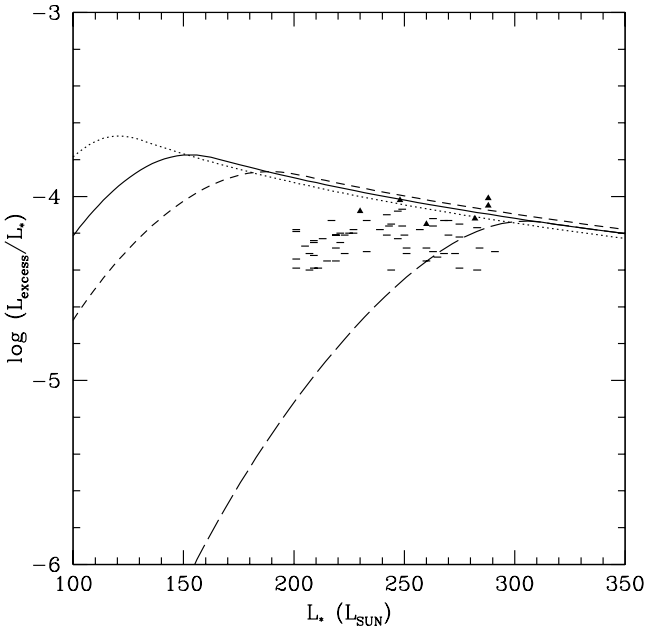

FIG. 3.—Solid curve shows a plot of log ($L_{\rm excess}/L_*$) vs. L_* for the standard model with both small and large KBOs described in the text with $D_{\rm init} = 45$ AU and $M_{\rm large}(0) = 0.1\ M_\oplus$. The dotted and dashed lines show calculations for the same parameters as the standard model, except that we use $D_{\rm init} = 40$ and 50 AU, respectively. The long-dashed line shows the results for the case with $D_{\rm init} = 45$ AU and only large KBOs for $M_{\rm big}(0) = 0.02\ M_\oplus$. We also display data for 66 stars identified by a procedure described in the text. The bars represent stars for which $f_{\rm ex}(25)$ defined by equation (46) is less than 0.1, while the triangles represent those stars for which $f_{\rm ex}(25) > 0.1$.

depth of interest here since in this case the infrared excess becomes detectable), the mean time between collisions of 3×10^6 yr is comparable to the Poynting-Robertson decay time for a dust particle of radius 100 μm orbiting around a red giant with a luminosity of 300 $L_\odot$. Therefore, as a very simple first approximation, grain-grain collisions are assumed to occur when the dust particle's orbital decay from the Poynting-Robertson drift has significantly changed its distance from the star. Although detailed calculations are required (see, for example, Wyatt et al. 1999; Krivov, Mann, & Krivova 2000), we adopt $D_{\rm final} = 0.5 D_{\rm init}$ as a crude representation of the effects of grain-grain collisions. Our results for the infrared excess luminosity are not strongly sensitive to this value for $D_{\rm init}/D_{\rm final}$, since from equation (44), $L_{\rm excess}$ depends only logarithmically on this ratio.

Using the calculations for $\dot{M}_{\rm KBO}$ described in § 3.5 and equation (44), we show in Figure 3 the results for $L_{\rm excess}/L_*$ as a function of L_* for several models. We see that $L_{\rm excess}/L_*$ increases until it reaches its maximum value, which occurs when $\Delta a \approx a_{\rm break}$. Models with initially some small KBOs and $a_{\rm break} = 1$ km show a higher value of $\dot{M}_{\rm KBO}$ than the model with only large KBOs and $a_{\rm break} = 200$ km. Once the star's luminosity is high enough that $\dot{M}_{\rm KBO}$ achieves saturation, then $L_{\rm excess}$ is approximately constant and $L_{\rm excess}/L_*$ decreases directly with L_*. From equations (30) and (44), the value for $L_{\rm excess}$ when $\dot{M}_{\rm KBO}$ reaches saturation is

$$L_{\rm excess} = \left[\frac{f_{\rm orbit}\ln(D_{\rm init}/D_{\rm final})}{8\ln(a_{\rm max}/a_{\rm break})}\right]\left(\frac{T_{\rm subl}}{T}\right) \times \left(1 + \frac{\dot{M}_{\rm wind}c^2}{L_*}\right)^{-1}\left[\frac{M_{\rm large}(0)c^2}{t_{\rm RGB}}\right]. \quad (45)$$

For the standard parameters adopted above, equation (45), which is an elaboration of equation (4) derived in § 2, yields $L_{\rm excess} \approx 0.02\ L_\odot$ when $T = 170$ K.

4. COMPARISON WITH OBSERVATIONS

In § 3, we have calculated the excess luminosity produced by a cloud of sublimating KBOs. We now show that this radiation may be detectable.

To measure the amount of excess radiation that a red giant exhibits at 25 μm, we need to determine its photospheric emission at this wavelength. Previous studies of first-ascent red giants have shown that the bulk of the detected flux at 12 μm, $F_\nu(12\ \mu{\rm m})$, emerges from the star's photosphere (see, for example, Jura, Webb, & Kahane 2001; Knauer, Ivezic, & Knapp 2001). (Here, we use the usual notation that ν denotes frequency.) We extrapolate from this measurement of the total flux at 12 μm to estimate the photospheric contribution to $F_\nu(25\ \mu{\rm m})$. From *IRAS* data, Jura (1999) found for the photospheres of the very brightest red giants that, on average, $F_\nu(25\ \mu{\rm m})/F_\nu(12\ \mu{\rm m}) = 0.233$. We define $f_{\rm ex}(25)$, the excess flux at 25 μm, by the expression

$$f_{\rm ex}(25) = \frac{1}{0.233}\frac{F_\nu(25\ \mu{\rm m})}{F_\nu(12\ \mu{\rm m})} - 1. \quad (46)$$

In Figure 4, we show a histogram of $f_{\rm ex}(25)$ for 66 nearby red giants identified by a procedure described below. Over 90% of the red giants exhibit $|f_{\rm ex}(25)| \leq 0.10$, implying that the *IRAS* data can be used to predict the photospheric flux at 25 μm to within 10%.

The histogram shown in Figure 4 is not symmetric around $f_{\rm ex}(25) = 0$. The sample of 66 stars from which the data are obtained has a mixture of surface gravities and abundances, and the intrinsic distribution of $f_{\rm ex}(25)$ around its mean value may be skewed. The skewed histogram might also result if some of these 66 stars possess an excess at 25 μm of $\sim$5% of the photospheric flux. Better data should allow us to confirm the reality of this hint of infrared excesses.

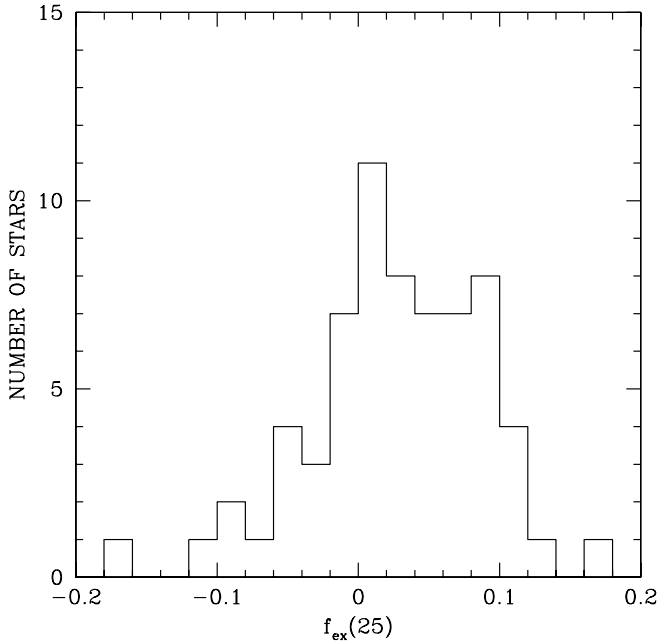

FIG. 4.—Histogram of the fractional excess at 25 μm, $f_{\rm ex}(25)$, defined in equation (35), for the stars represented in Figure 3.

The sample of stars is chosen from nearby red giants, which are least subject to interstellar extinction. We select stars from the the Yale Bright Star Catalog with $B-V \geq 1.0$ mag that also lie within 150 pc of the Sun (from *Hipparcos* data), have $M_V \leq 0.0$ mag, and have 200 $L_\odot < L < 300$ $L_\odot$. We use 200 $L_\odot$ as the lower bound of the luminosities that we consider, because, as shown in Figure 3, for stellar luminosities lower than this value, the amount of the infrared excess becomes very sensitive to the initial numbers of KBOs smaller in radius than 200 km. We use 300 $L_\odot$ as the upper bound for the stellar luminosity, because for luminosities higher than this value, equation (44) begins to overestimate the infrared excess as Δa approaches $a_{\max}$. We compute the star's luminosity by assuming no reddening and applying the bolometric corrections from Flower (1996) for red giants with the assumption that $M_{\rm bol}(\odot) = 4.74$ mag (Bessell, Castelli, & Plez 1998). There are 66 stars that satisfy these criteria and that were detected with IRAS.

In our models described in § 3, $D_{\rm final} = 0.5 D_{\rm init}$. Because this change in orbital radius is relatively small, we assume that the grains emit at a single temperature determined from equation (16) by their initial distance from the star. Assuming that the infrared excess is characterized by a 170 K blackbody, then $L_{\rm excess} \approx 1.5 \nu L_\nu(25)$, where $L_\nu(25)$ denotes the specific luminosity at 25 μm.

In Figure 3, in addition to showing the calculations for the standard model of $L_{\rm excess}/L_*$ versus L_*, we also plot the data for the 66 identified red giants. For each star, we use its distance and the non–color corrected flux from the *IRAS* Faint Source Catalog or, when that is not available, the flux from the Point Source Catalog, to estimate $L_\nu(25)$. For the stars with $f_{\rm ex}(25) < 0.1$, we plot with a horizontal bar the quantity $(0.1)(1.5)\nu L_\nu(25\ \mu{\rm m})/L_*$ versus L_*. For stars with $f_{\rm ex}(25) > 0.10$, we plot with a filled triangle the quantity $f_{\rm ex}(25)(1.5)\nu L_\nu(25\ \mu{\rm m})/L_*$ versus L_*. Of the six stars with $f_{\rm ex}(25) > 0.1$, there are three stars, HR 736, HR 7956, and HR 9029, that also have 60 μm excesses. The 60 μm excess for HR 9029 has also been noted by Plets et al. (1997). These infrared excesses are so small that it is very difficult to infer a dust temperature, and this evidence is, at best, a weak hint that these stars possess sublimating KBOs.

From Figure 3, we see that the data points usually lie below the theoretical curve for the regime for which initially there are many KBOs smaller than 200 km in radius. Therefore, we find that the production of dust from systems containing comet-like bodies can produce a detectable infrared excess if the total mass of the KBOs is at least 0.1 $M_\oplus$. We can also see from Figure 3 that if initially there are only KBOs with a radius larger than 200 km, then a KBO system similar to that in our own solar system would not produce a detectable infrared excess around most red giants. However, this calculation was performed with $M_{\rm big}(0) = 0.02$ $M_\oplus$. If, instead, we assume that $M_{\rm big}(0) \approx 0.1$ $M_\oplus$, then the predicted fluxes would be a factor of 5 larger than shown. In this case, the data points would then lie below the computed line, and an infrared excess would be detectable. Thus, as anticipated in our discussion in § 2, regardless of the exact size distribution, we expect that an infrared excess might be detectable if the total mass of the KBO system lying at 45 AU orbital radius is larger than 0.1 $M_\oplus$.

5. DISCUSSION

Our main argument is that as a star evolves during the red giant phase, it is possible to constrain the mass of the KBOs in the system. Here, we consider how our results compare with other investigations of the outer regions of our solar system and its analogs among other stars.

While sublimation of KBOs at an orbital radius of 45 AU might lead to a detectable infrared excess during a star's red giant evolution, our analysis does not provide strong constraints on the mass of KBOs much further than 50 AU. Melnick et al. (2001), Ford & Neufeld (2001), and Ford et al. (2003) have proposed that, in order to account for the detected circumstellar H_2O and OH around the mass-losing carbon star IRC +10216, there is a cloud of comets at $\sim$300 AU with a mass of at least $\sim$10 $M_\oplus$. In contrast, our typical upper limit to the mass in comet-like objects is $\sim$0.1 $M_\oplus$ at $\sim$45 AU. This apparent mass gradient of KBOs is remarkable and deserves further study.

Main-sequence stars often possess from 0.01 to 0.1 $M_\oplus$ of dust at orbital separations of typically between 10 and 100 AU (see Zuckerman 2001). Our results for evolving red giants are consistent with the hypothesis that there may be as much as an additional $\sim$0.1 $M_\oplus$ in icy comets closer than $\sim$50 AU around most main-sequence stars. However, it appears that macroscopic KBOs with radii greater than 1 km do not overwhelmingly dominate the mass budgets of solid material orbiting beyond 10 AU around those main-sequence stars with measured amounts of dust.

The total mass of the KBOs in orbit around our Sun is somewhere between 0.01 and 0.1 $M_\oplus$. Even the larger value is much less mass than predicted by extrapolations from the inner solar system for the initial solar nebula (Luu & Jewitt 2002). Our upper limits for the mass of systems of KBOs around red giants shows that the analogs to the Kuiper Belt also have similarly "low" masses at orbital radii less than 50 AU.

Very precise measurements of the fluxes from red giants in comparison with model atmospheres may allow for a more reliable determination of whether they possess infrared excesses. If the photospheric flux could be estimated to within 1%, instead of 10%, it would be possible to improve estimates of the masses of the KBO systems by a factor of 10. We could then determine whether some stars have KBO systems of $\sim$0.1 $M_\oplus$.

In this paper, we have focused on the production of an infrared excess by sublimation of comets. Our calculations do not pertain to those red giants for which an infrared excess with a characteristic dust temperature of $\sim$70 K is measured, which is produced by $\sim$0.1 $M_\oplus$ of dust at $\sim$200 AU from the star (Jura 1999). The origin of this dust is uncertain; at least in some cases, confusion with interstellar cirrus is possible. Further work is required to understand the nature of this material.

6. CONCLUSIONS

We have computed the evolution of a system of KBOs after a star becomes a red giant. For KBOs at 45 AU from the host star, we find that the dust released during the sublimation of ice from these objects might produce a detectable infrared excess around red giants of luminosities in the range 200 to 300 $L_\odot$, if the mass of the KBOs is at least 0.1 $M_\oplus$. To date, there is no strong evidence for such sublimating KBOs, but with improved data, it may be possible to detect systems that are analogs to our solar system around first-ascent red giants.

This work has been partly supported by NASA.

REFERENCES

Abramowitz, M., & Stegun, I. A. 1965, Handbook of Mathematical Functions (New York: Dover)
Artymowicz, P. 1988, ApJ, 335, L79
Bernstein, G. M., Trilling, D. E., Allen, R. L., Brown, M. E., Holman, M., & Malhotra, R. 2003, AJ, submitted
Bessell, M. S., Castelli, F., & Plez, B. 1998, A&A, 333, 231
Burns, J. A., Lamy, P. L., & Soter, S. 1979, Icarus, 40, 1
Flower, P. J. 1996, ApJ, 469, 355
Ford, K. E. S., & Neufeld, D. A. 2001, ApJ, 557, L113
Ford, K. E. S., Neufeld, D. A., Goldsmith, P. F., & Melnick, G. J. 2003, ApJ, 589, 430
Girardi, L., Bressan, A., Bertelli, G., & Chiosi, C. 2000, A&AS, 141, 371
Greenberg, J. M. 1998, A&A, 330, 375
Gustafson, B. A. S. 1994, Annu. Rev. Earth Planet. Sci., 22, 553
Hanner, M. S., Veeder, G. J., & Tokunaga, A. T. 1992, AJ, 104, 386
Harker, D. E., Wooden, D. H., Woodward, C. E., & Lisse, C. M. 2002, ApJ, 580, 579
Judge, P. G., Jordan, C., & Rowan-Robinson, M. 1987, MNRAS, 224, 93
Jura, M. 1990, ApJ, 365, 317
———. 1999, ApJ, 515, 706
Jura, M., Webb, R. A., & Kahane, C. 2001, ApJ, 550, L71
Kenyon, S. J. 2002, PASP, 114, 265
Kenyon, S. J., & Windhorst, R. A. 2001, ApJ, 547, L69
Kim, S. S., Zuckerman, B., & Silverstone, M. 2001, ApJ, 550, 1000
Kirsch, T., Baade, R., & Reimers, D. 2001, A&A, 379, 925
Knauer, T. G., Ivezic, Z., & Knapp, G. R. 2001, ApJ, 552, 787
Krivov, A. V., Mann, L., & Krivova, N. A. 2000, A&A, 362, 1127
Kyte, F., & Wasson, J. 1986, Science, 232, 1225
Li, A., & Greenberg, J. M. 1998, ApJ, 498, L83
Love, S. G., & Brownlee, D. E. 1995, Science, 262, 550
Luu, J. X., & Jewitt, D. C. 2002, ARA&A, 40, 63
McDonnell, J. A. M., et al. 1987, A&A, 187, 719
Melnick, G. J., Neufeld, D. A., Ford, K. E. S., Hollenbach, D. J., & Ashby, M. L. N. 2001, Nature, 412, 160
Plets, H., Waelkens, C., Oudmaijer, R. D., & Waters, L. B. F. M. 1997, A&A, 323, 513
Robinson, R. D., Carpenter, K. G., & Brown, A. 1998, ApJ, 503, 396
Smith, G. 1998, PASP, 110, 1119
Stern, S. A., Shull, J. M., & Brandt, J. C. 1990, Nature, 345, 305
Teplitz, V. L., Stern, S. A., Anderson, J. D., Rosenbaum, D., Scalise, R. J., & Wentzler, P. 1999, ApJ, 516, 425
Wyatt, M. C., Dermott, S. F., Telesco, C. M., Fisher, R. S., Grogan, K., Holmes, E. K., & Pina, R. K. 1999, ApJ, 527, 918
Zolensky, M. E., et al. 1995, Adv. Space Res., 16, 53
Zuckerman, B. 2001, ARA&A, 39, 549
Zuckerman, B., Kim, S. S., & Liu, T. 1995, ApJ, 446, L79